Using Advanced Analytical Techniques to Classify New Meteorites

M Hammett, Plymouth University, Drake Circus, Plymouth, Devon, PL4 8AA, UK

In the first of our featured RMS Summer Studentship reports, Megan Hammett of Plymouth University employs advanced petrologic techniques to contribute new data to ongoing asteroid research

Meteorites are classified in order to broadly sort similar types (Bischoff, 2001); with the conclusive goal to better understand the origin of these extraterrestrial rocks and the relationships they bear to their parent bodies (McSween, 2000). Classification inaugurated in the 1860s; when Rose divided samples into 'chondrites' and 'achondrites' and Maskelyne categorised three types – stony, iron and stony-iron (Weisburg, McCoy and Krot, 2006). However, classification evolves as more data is obtained and new meteorites are discovered. Today, classification is largely based on meteorites' mineralogical and petrographic characteristics and whole-rock chemical and O-isotopic compositions; albeit petrologic examinations largely supersede bulk chemical studies as the primary classification methods, owed to their simplicity (Weisburg, McCoy and Krot, 2006). This study utilises advanced petrologic techniques to classify new meteorite samples, in order to contribute data to our extensive existing meteorite collection and thus, ongoing asteroid research.

Classification Methods

Modern meteorite classification defines two broad divisions – 'differentiated' and 'un-differentiated' (Bischoff, 2001) – more commonly recognised as chondrites and achondrites, respectively (Weisburg, McCoy and Krot, 2006). Primitive achondrites are a subdivision located between chondrites and achondrites; however, the genetic relationship they bear to existing groups of chondritic meteorites remains controversial (Weisburg, McCoy and Krot, 2006). These subdivisions are further separated into groups, and closely related groups are additionally split into subgroups and clans as need be. Closely related groups or clans are in turn referred to as classes; however, this is most common practice for chondrites, with little agreement on how achondrites fit into the scheme (Weisburg, McCoy and Krot, 2006). The classification hierarchy is summarised below (Figure 1).

Petrologic investigations initially differentiate chondrites from achondrites based on texture. Chondrites have characteristic aggregational textures, consisting largely of chondrules and calcium-aluminium inclusions (CAI's) in a dark matrix (McSween, 2000), whereas achondrites exhibit those of igneous and/or recrystallisation processes (Weisburg, McCoy and Krot, 2006). Petrologic methods then classify samples through evaluation of modal abundances and mineral compositions, alongside chondrule size and chondrule to matrix ratios for chondrites (Weisburg, McCoy and Krot, 2006). All chondrites are assigned a number according to their petrologic type (Figure 2), related to the grade of metamorphism they have undergone (McSween, 2000). Types 1 and 2 represent an increasing degree of hydrous alteration; type 3.0 represents unmetamorphosed materials, with successive numbers indicating increasing petrologic equilibration and recrystallisation; type 7 indicates chondrites that have been completely recrystallised (Weisburg, McCoy and Krot, 2006). The chemical-petrological classification scheme used in this study is included (Table 1). Chondrites are also assigned values for the degree of shock metamorphism (S1-S6) and terrestrial weathering (W1-W6) they have experienced. These are based on the petrographic features of silicate minerals (i.e. olivine, pyroxene and plagioclase) (Weisburg, McCoy and Krot, 2006) and oxidation of metals and sulphides (Wlotzka, 1993), respectively.

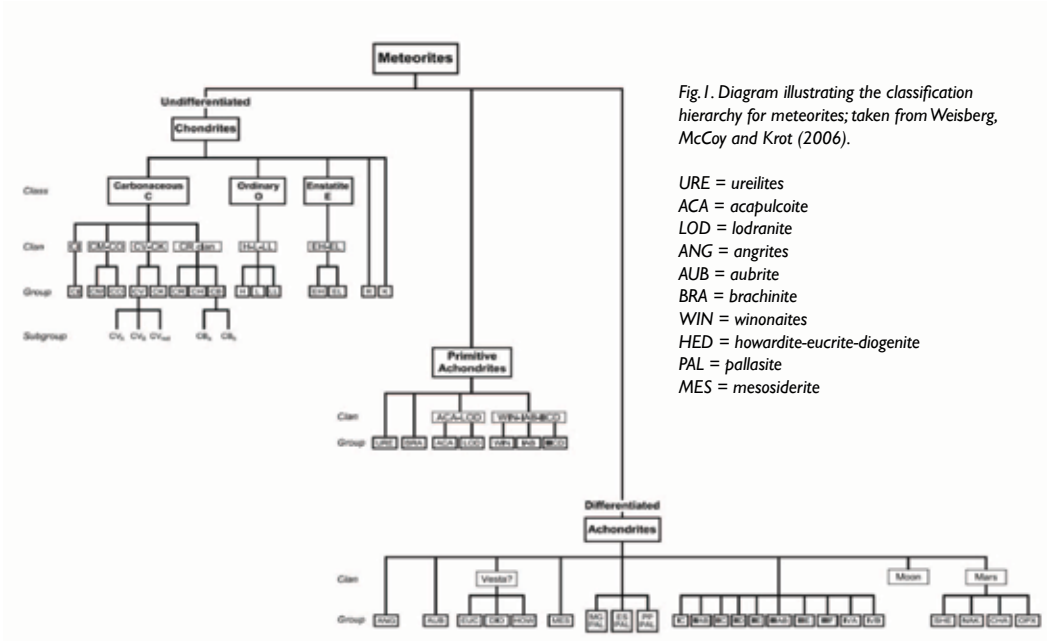

Fig.1. Diagram illustrating the classification hierarchy for meteorites; taken from Weisberg, McCoy and Krot (2006).

URE = ureilites
ACA = acapulcoite
LOD = lodranite
ANG = angrites
AUB = aubrite
BRA = brachinite
WIN = winonaites
HED = howardite-eucrite-diogenite
PAL = pallasite
MES = mesosiderite

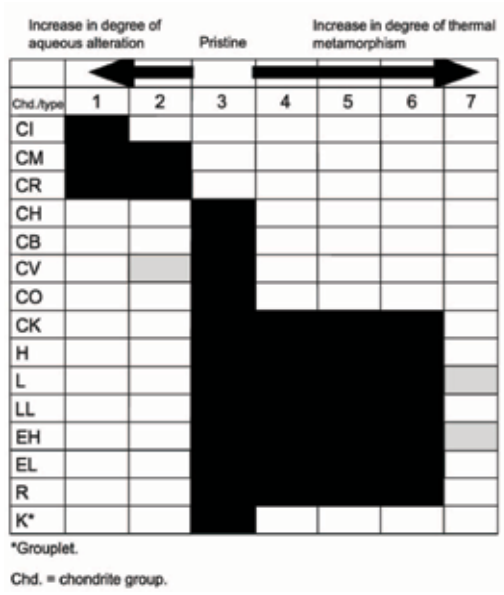

Fig.2. Diagram highlighting the petrologic types of each chondrite group; taken from Weisberg, McCoy and Krot (2006).

Samples and Analytical Techniques

Five meteorite thin sections were prepared prior to analysis; 18512E, 94131, 19414C, 22414B and 25418B. Numbers denote the date on which each meteorite was discovered and letters the order in which samples were found (ie. E is the fifth sample collected that day). Samples vary in size from 2.5-3.5 cm; thus, the resolution of each analysis was varied as required.

Data acquisition was conducted at the University of Plymouth, UK. Preliminary textural and mineralogical investigations were carried out using a polarising microscope; subsequent data was obtained at the Plymouth Electron Microscopy Centre with a JEOL 7001 Field Emission SEM. The SEM equipment uses a Schottky electron gun, and combined with the running of AZTEC software, allows chemical mapping (EDS) analysis of the samples to determine the chemical composition and elemental dispersion. SEM images were additionally taken using this equipment; as were large area maps to analyse the modal abundances of each entire section at high resolution. Modal analysis additionally required the use of Adobe Photoshop.

Results

18512E:

Petrological Description

The meteorite has a chondritic texture with a fine-grained, barely recrystallised matrix. Chondrules are predominantly well-rounded with distinct edges and contain fine-grained mesostasis; many are rimmed or traversed by iron oxide (Figures 3a-c). They vary significantly in both size (0.2-2.5 mm) and composition – observable textures include RP, BO (Figure 3d), PO, PP, POP (Figure 3e) and GO. Notably, in multiple POP chondrules, olivine is poikilitically enclosed in low-Ca pyroxene. The

Criterion	1	2	3	4	5	6	7
Homogeneity of olivine compositions	—	>5% mean deviations		≤5%	Homogeneous		
Structural state of low-Ca pyroxene	—	Predominantly monoclinic		>20% monoclinic	≤20% monoclinic	Orthorhombic	
Feldspar	—	Minor primary grains		Secondary <2-μm grains	Secondary 2–50-μm grains	Secondary >50-μm grains	
Chondrule glass	Altered or absent	Mostly altered, some preserved	Clear, isotropic	Devitrified	Absent		
Metal: Maximum Ni (wt%)	—	<20 taenite minor or absent	>20 kamacite and taenite in exsolution relationship				
Sulfides: Mean Ni (wt%)	—	>0.5	<0.5				
Matrix	Fine grained opaque	Mostly fine-grained opaque	Opaque to transparent	Transparent, recrystallized			
Chondrule-matrix integration	No chondrules	Sharp chondrule boundaries		Some chondrules can be discerned, fewer sharp edges	Chondrules poorly delineated	Primary textures destroyed	
Carbon (wt%)	3–5	0.8–2.6	0.2–1	<0.2			
Water (wt%)	18–22	2–16	0.3–3	<1.5			

Table. 1. Summary of criteria required for classification of the petrologic type of chondrites; taken from Weisberg, McCoy and Krot (2006), based on the original scheme by Van Schmus and Wood (1967).

main phases are low-Ca pyroxene and olivine; minor phases are plagioclase, high-Ca pyroxene and troilite; accessory phases are chromite, apatite, oldhamite and quartz. There is a high abundance of metallic iron, albeit ~98% of metal grains are almost completely oxidised. Several low-Ca pyroxene grains exhibit Ca-rich rims and exsolution lamellae of variable thicknesses (Figure 3f). Olivine displays distinctive curved fracturing, many filled by iron oxide, and strong mosaicism is common in grains. There is no shock melting.

Geochemical Description

Olivine Fo76.7-81.7 Fa18.3-23-3, mean = Fo74.1 Fa20.8, std = Fo1.6 Fa1.4, n = 10; Low-Ca pyroxene Wo0.0-5.0 En78.2-82.5 Fs14.6-21.4, mean = Wo3.4 En 78.8 Fs17.9, std = Wo1.9 En1.5 Fs1.8, n = 10; High-Ca pyroxene Wo17.7-52.5 En34.1-55.5 Fs0.0-41.1, mean = Wo29.4 En54.2 Fs16.4, std = Wo10.5 En7.0 Fs13.0, n = 10; Feldspar An0.0-100 Ab0.0-100, mean = An52.0 Ab48.0, std = An42.4 Ab42.4, n = 10.

Classification

Ordinary chondrite (H4, S4, W4). 94131:

Petrological Description

The meteorite has a chondritic texture with a fine-grained, barely recrystallised matrix. Chondrules are predominantly well-rounded with distinct edges and contain fine-grained mesostasis; they vary significantly in both size (0.4-1.2 mm) and composition – observable textures include RP, BO, PO, PP, POP and C (Figures 4a-e). The main phases are low-Ca pyroxene and olivine; minor phases are plagioclase and high-Ca pyroxene; accessory phases are troilite, chromite, apatite and oldhamite. There is a high abundance of metallic iron, albeit ~95% of metal grains are almost completely oxidised. Several low-Ca pyroxene grains exhibit Ca-rich rims and exsolution lamellae of variable thicknesses. Minor plagioclase grains exhibit both simple and lamellar twinning and symplectitic textures are present. Olivine displays distinctive curved fracturing, many are filled by iron oxide, alongside strong

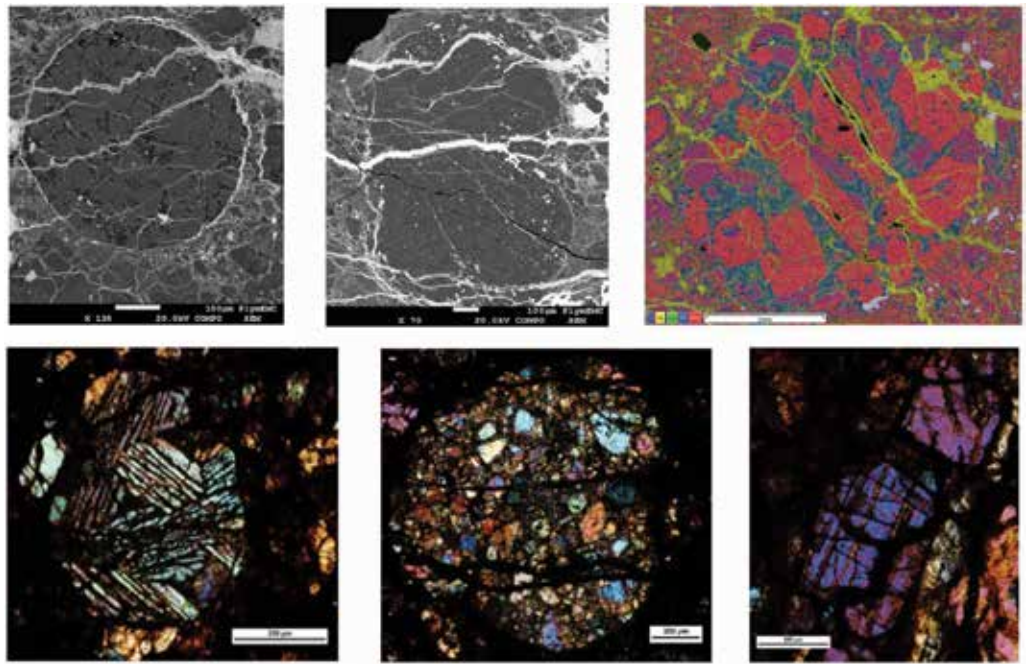

Fig.3. (a) SEM image of a well-rounded, well-defined POP chondrule rimmed by iron oxide. (b) SEM image of a well-defined compound RP chondrule; note the rims of iron oxide, which also traverses the chondrules. (c) False coloured element map of a well-defined, well-rounded POP chondrule. (d) XPL optical microscope image of a well-rounded BO chondrule exhibiting parallel bars of olivine orientated in various directions. (e) XPL optical microscope image of a well-defined, well-rounded POP chondrule. (f) XPL optical microscope image of a pyroxene grain displaying exsolution lamellae.

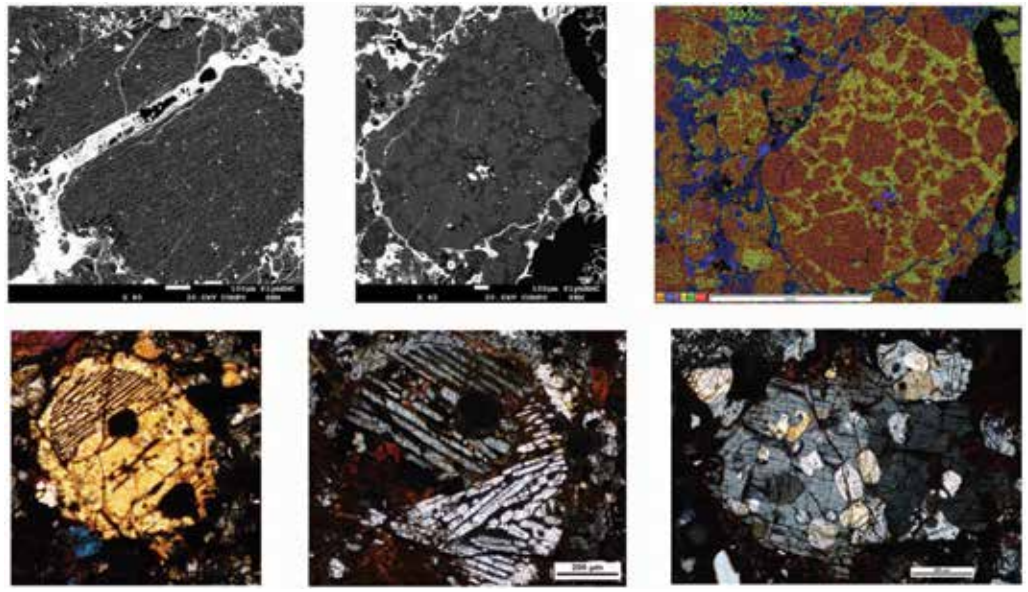

Fig.4. (a) SEM image of a well-defined BO chondrule composed of thin, parallel olivine laths; iron oxide traverses through. (b) SEM image of a well-defined PO chondrule. (c) False coloured element map of the same PO chondrule, alongside a smaller (0.4 mm) PP chondrule (left). (d) XPL optical microscope image of a BO chondrule; mostly all olivine shell. (e) XPL optical microscope image of a BO chondrule consisting of parallel bars of olivine orientated in various directions; note the abnormally low birefringence. (f) XPL optical microscope image of a poikilitic olivine crystal exhibiting strong planar deformation fractures and abnormally low birefringence; inclusion grains are orthopyroxene.

planar deformation fractures and abnormally low birefringence (Figures 4e and 4f); suggestive of a highly shocked condition. Notably, there is no shock melting.

Geochemical Description

Olivine Fo73.9-81.4 Fa18.6-26.1, mean = Fo78.8 Fa21.2, std = Fo2.0 Fa2.0, n = 10; Low-Ca pyroxene Wo0.0-12.4 En72.4-83.1 Fs15.3-23.6, mean = Wo6.58 En74.5 Fs19.0, std = Wo4.3 En3.8 Fs2.7, n= 10; High-Ca pyroxene Wo22.2-56.9 En43.1-59.3 Fs0-18.5, mean = Wo43.2 En46.6 Fs10.2, std = Wo11.3 En5.7 Fs6.8, n = 7; Feldspar An0-47.8 Ab52.2-100, mean = An34.4, Ab35.6, std = An13.6 Ab25.4, n = 10.

Classification

Ordinary chondrite (H4, S5, W3). 19414C:

Petrological Description

The meteorite has a chondritic texture with a substantially recrystallised matrix consisting of coarse mineral grains. Chondrules are poorly delineated and have begun integrating with the surrounding mineral grains; several appear remnant (Figures 5a-c). Those discernible contain fine-grained mesostasis and vary significantly in both size (0.3-2.5 mm) and composition – observable textures are RP, BO, OP and POP. Notably, there is a 2.5 mm BO chondrule with a partially defined boundary; however, it exhibits significant alteration also (Figure 5d). The main phases are olivine and low-Ca pyroxene; minor phases are plagioclase (Na-rich) and high-Ca pyroxene and troilite; accessory phases are chromite and apatite. There is a moderately low abundance of metallic iron and ~50% of metal grains are almost completely oxidised (Figure 5e). Olivine grains exhibit distinctive curved fractures, many filled by iron oxide, and mosaicism is observed in several (Figure 5f). There is no shock melting.

Geochemical Description

Olivine Fo69.2-78.2 Fa21.8-30.8, mean = Fo74.1 Fa25.9, std = Fo2.6 Fa2.6, n = 10; Low-Ca pyroxene Wo0-.0-3.8 En71.7-79.9 Fs21.3-28.3, mean = Wo2.4 En74.1 Fs 23.6, std = Wo1.3 En2.3 Fs2.6, n = 10; High-Ca pyroxene Wo31.6-64.7 En35.4-54.4 Fs0.0-18.0, mean = Wo43.2 En43.3 Fs13.5, std = Wo8.6 En6.4 Fs7.9, n = 10; Feldspar An0.0-35.5 Ab64.5-100,

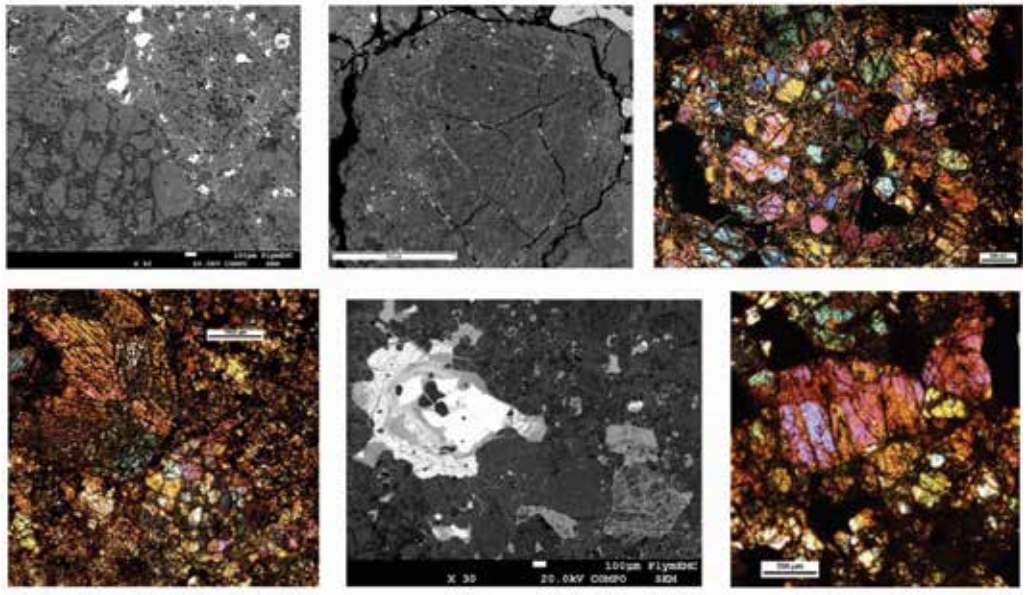

Fig.5. (a) SEM image of two poorly defined POP chondrules; note their integration with the surrounding mineral grains, particularly the upper right chondrule. (b) SEM image of a remnant RP chondrule composed of low-Ca pyroxene. (c) XPL optical microscope image of a poorly defined POP chondrule; note its integration with the surrounding mineral grains. (d) XPL optical microscope image of a partially defined BO chondrule and a PO chondrule; both show significant alteration and integration with the surrounding mineral grains. (e) SEM image of various metallic iron and sulphide phases. (f) XPL optical microscope image of an olivine grain exhibiting mosaicism.

mean = An17.1 Ab82.9, std = An13.0 Ab13.0, n = 10.

Classification

Ordinary chondrite (L6, S4, W2). 22414B:

Petrological Description

The meteorite has a chondritic texture with a fine-grained, moderately recrystallised matrix. Several chondrules can be discerned, however, most lack sharp well-defined edges; the matrix is difficult to distinguish from these (Figures 6a-c). Chondrules contain fine-grained mesostasis and vary significantly in both size (0.15-2 mm) and composition – observable textures include RP, BO, PO, PP, POP and C. Notably, there are two anomalous well-rounded, Al-rich chondrules (Figure 6d); formed of Na-rich plagioclase that becomes increasingly Ca-rich towards the rims. The main phases are olivine and low-Ca pyroxene; minor phases are plagioclase (Na-rich), high-Ca pyroxene and troilite; accessory phases are chromite and apatite. There is a low abundance of metallic iron and ~95% of metal grains have been almost completely oxidised. Several low-Ca pyroxene grains exhibit simple twinning and exsolution lamellae of variable thicknesses (Figure 6e). Olivine displays distinctive curved fracturing, commonly filled by iron oxide, with strong mosaicism observed in several grains (Figure 6f).

Geochemical Description

Olivine Fo75.3-100 Fa0-24.7, mean = Fo78.5 Fa21.5, std = Fo7.4 Fa7.4, n = 10; Low-Ca pyroxene Wo0.0-6.1 En70.9-84.3 Fs15.7-24.0, mean = Wo4.41 En75.6 Fs20.0, std = Wo2.1 En3.9 Fs2.7, n = 10; High-Ca pyroxene Wo19.7-53.7 En45.0-60.6 Fs0.0-19.7, mean = Wo35.7 En48.5 Fs15.9, std = Wo17.6 En8.6 Fs9.9, n = 3; Feldspar An11.6-100 Ab0.0-88.3, mean = An38.9 Ab61.1, std = An33.8 Ab33.8, n = 10.

Classification

Ordinary chondrite (L5, S4, W3). 25418B:

Petrological Description

The meteorite has a chondritic texture, although appears to contain two separate lithologies; one with a fine-grained, moderately recrystallised matrix (A) and another with a substantially recrystallised matrix consisting of coarse mineral grains (B). Comprehensively, several chondrules can be discerned; however, most lack sharp well-defined edges and are difficult to distinguish from the remaining matrix (Figures 7a and 7b). Discernible chondrules contain fine-grained mesostasis and vary significantly in both size (0.7-2.5 mm) and

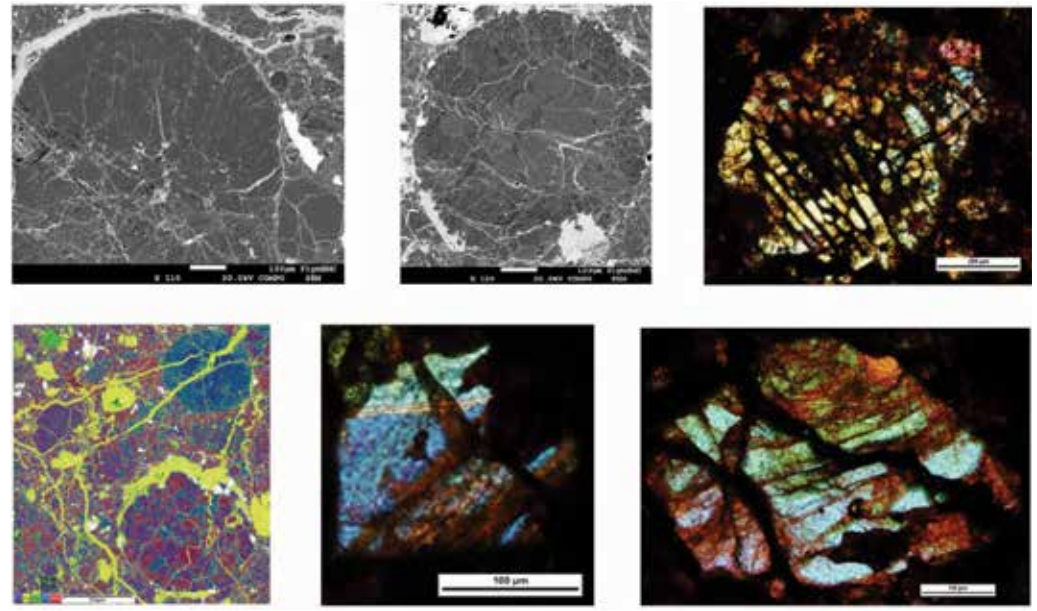

Fig.6. (a) SEM image of an RP chondrule, composed of low-Ca pyroxene, where half can be discerned and the other is difficult to distinguish from the remaining matrix. (b) SEM image of a discernible POP chondrule; it does, however, show significant alteration and iron oxide weathering. (c) XPL optical microscope image of a BO chondrule exhibiting moderate alteration. (d) False colour element map showing an anomalous well-rounded, Al-rich chondrule (top right) and a discernible POP chondrule (bottom right). (e) XPL optical microscope image of a low-Ca pyroxene grain exhibiting both simple twinning and exsolution lamellae. (f) XPL optical microscope image of an olivine grain displaying strong mosaicism.

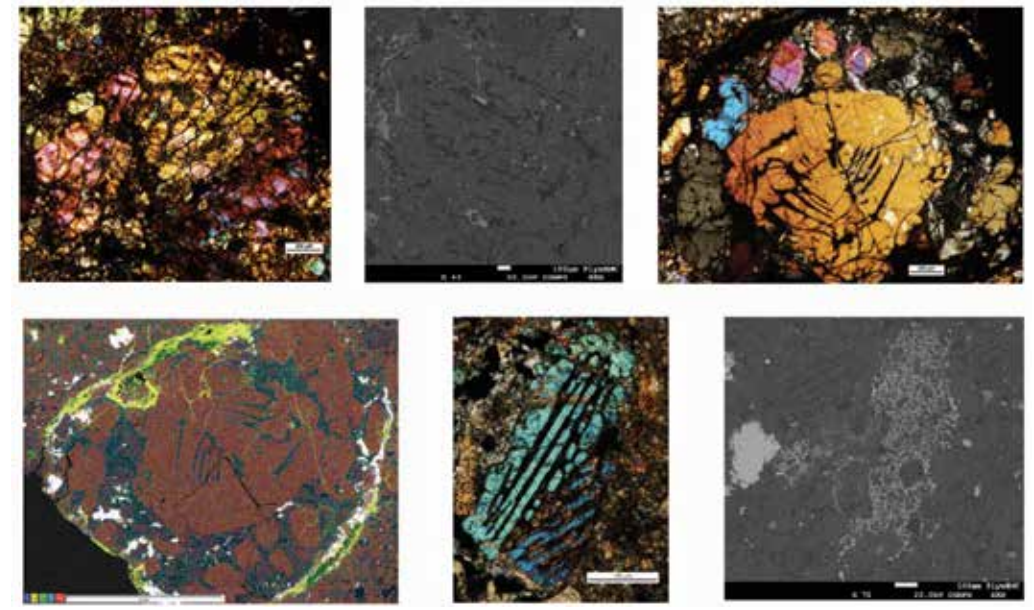

Fig.7. (a) XPL optical microscope image of a poorly defined BO chondrule exhibiting moderate alteration. (b) SEM image of a BO chondrule that lacks well-defined edges. (c) XPL optical microscope image of a discernible POP; note the planar deformation fractures on the large, well-formed olivine crystals. (d) False colour element map of the above POP chondrule; here you can see its discontinuous rim of iron oxide. (e) XPL optical microscope image of a compound BO chondrule; mostly all olivine shell. (f) SEM image of disseminated melt pocket composed of both iron sulphide and oxide.

composition – observable textures include POP (Figures 7c and 7d), PO and BO (Figure 7e). The main phases are olivine and low-Ca pyroxene; minor phases are plagioclase (Na-rich), high-Ca pyroxene and troilite; accessory phases are chromite and chlorapatite. There is a very low abundance of metallic iron; although within lithology A ~30% of metal grains have been almost completely oxidised, whereas within lithology B ~95% of metal grains have been affected. Several low-Ca pyroxene grains exhibit exsolution lamellae of variable thicknesses. Minor plagioclase grains exhibit both simple and lamellar twinning. Olivine displays distinctive curved fracturing, many filled by iron oxide, alongside strong planar deformation fractures in several grains; suggestive of a highly shocked condition. There is no evidence of extensive shock melting; however, there is a small (1x1 mm) disseminated melt pocket composed of both iron sulphide and oxide (Figure 7f), and a postulated igneous melt clast.

Geochemical Description

Olivine Fo64.9-71.6 Fa28.4-35.1, mean = Fo68.5 Fa31.5, std = Fo2.0 Fa2.0, n = 10; Low-Ca pyroxene Wo0.0-3.13 En63.9-77.4 Fs22.6-33.9, mean = Wo2.8 En67.0 Fs28.3, std = Wo1.4 En4.0 Fs3.6, n = 11; High-Ca pyroxene Wo33.3-57.4 En38.1-49.7 Fs0.0-28.6, mean = Wo42.4 En41.4 Fs16.3, std = Wo7.0 En3.6 Fs9.4, n = 10; Feldspar An0.0-100 Ab0.0-100, mean = An22.4 Ab68.0, std = An30.9 Ab30.9, n = 10.

Classification

Ordinary chondrite (LL5, S5, W2-3).

Conclusion

The continued classification of new meteorites allows our existing knowledge and techniques to evolve and grow. This is critical in achieving the ultimate goal of understanding the origin of meteorites and the prominence of their parent bodies in the solar system. This study has classified five new meteorites through the comprehensive application of several non-destructive, advanced analytical techniques. All five samples were classified as ordinary chondrites, based largely on their mineralogical and petrographic characteristics; and examples of all ordinary chondrite groups were identified. As more samples are discovered and investigated classification will evolve further; in turn, driving asteroid research towards its conclusive goals.

Acknowledgements

This study was funded by the Royal Microscopy Society as a Summer Studentship, and for this I would like to extend my upmost gratitude. I would also like to thank my supervisor, Dr Natasha Stephen, for her patience and exceptional guidance during this project; as well as all the technical staff at the Plymouth Electron Microscopy Centre for their support throughout.

References

Bischoff, A. (2001). Meteorite classification and the definition of new chondrite classes as a result of successful meteorite search in hot and cold deserts. Planetary and Space Science, 49(8), pp.769-776.

McSween, H. (2000). Meteorites and their parent planets. Cambridge [u.a.]: Cambridge Univ. Press.

Weisberg, M. K., McCoy, T. J. & Krot, A. N. (2006). Systematics and Evaluation of Meteorite Classification. In D. S. Lauretta, L. A. Leshin, & H. Y. Jr. McSween (Eds.), Meteorites and the Early Solar System II, Tucson: The University of Arizona Press, pp.19-52.

Van Schmus, W. and Wood, J. (1967). A chemical-petrologic classification for the chondritic meteorites. Geochimica et Cosmochimica Acta, 31(5), pp.747-765 (quoted in Weisberg, McCoy and Krot, 2006). Wlotzka, F. (1993). A weathering scale for the ordinary chondrites. Meteoritics, 23(3), pp.460.

Megan Hammett
Plymouth University